



# Mathematic model and tooth contact analysis of a new spiral non-circular bevel gear

HAN Xing-hui(韩星会), ZHANG Xuan-cheng(张轩诚), ZHENG Fang-yan(郑方焱)\*,  
XU Man(徐曼), TIAN Jun(田俊)

School of Automotive Engineering, Hubei Key Laboratory of Advanced Technology of Automotive Parts,  
Wuhan University of Technology, Wuhan 430070, China

© Central South University 2022

**Abstract:** A novel spiral non-circular bevel gear that could be applied to variable-speed driving in intersecting axes was proposed by combining the design principles of non-circular bevel gears and the manufacturing principles of face-milling spiral bevel gears. Unlike straight non-circular bevel gears, spiral non-circular bevel gears have numerous advantages, such as a high contact ratio, high intensity, good dynamic performance, and an adjustable contact region. In addition, while manufacturing straight non-circular bevel gears is difficult, spiral non-circular bevel gears can be efficiently and precisely fabricated with a 6-axis bevel gear cutting machine. First, the generating principles of spiral non-circular bevel gears were introduced. Next, a mathematical model, including a generating tooth profile, tooth spiral, pressure angle, and generated tooth profile for this gear type was established. Then the precision of the model was verified by a tooth contact analysis using FEA, and the contact patterns and stress distributions of the spiral non-circular bevel gears were investigated.

**Key words:** non circular gear; spiral bevel gear; mathematic model; tooth contact analysis (TCA)

**Cite this article as:** HAN Xing-hui, ZHANG Xuan-cheng, ZHENG Fang-yan, XU Man, TIAN Jun. Mathematic model and tooth contact analysis of a new spiral non-circular bevel gear [J]. Journal of Central South University, 2022, 29(1): 157–172. DOI: <https://doi.org/10.1007/s11771-022-4898-8>.

## 1 Introduction

Non-circular gears can be categorized according to the relationships of their axes as either non-circular cylindrical gears, which have parallel axes, and non-circular bevel gears, which have intersecting axes. While non-circular cylindrical gears are used in function generators [1, 2], gear pumps [3, 4], and a variety of other mechanical systems [5–8], non-circular bevel gears are often

applied to high-order ellipse bevel gear pumps [9], variable ratio differentials [10, 11], and other functional generators [12].

Non-circular gears can be categorized further as straight non-circular gears and spiral, or helical, non-circular gears based on the longitudinal geometrical shapes of their corresponding gear teeth. While previous studies concerning non-circular cylindrical gears have considered both straight and spiral gear types, studies concerning non-circular bevel gears have concentrated on

**Foundation item:** Project(52175361) supported by the National Natural Science Foundation of China; Project(2019CFA041) supported by the Natural Science Foundation of Hubei Province, China; Project(WUT: 202407002) supported by the Fundamental Research Funds for the Central Universities, China

**Received date:** 2021-05-08; **Accepted date:** 2021-09-15

**Corresponding author:** ZHENG Fang-yan, PhD, Associated Professor; E-mail: 382280761@qq.com; ORCID: <https://orcid.org/0000-0003-4249-9199>

straight gear types.

For example, OLLSON [13] proposed that gear types can be used to implement the driving of intersecting axes. In addition, XIE et al [14] presented a functional mapping method for the tooth profiles of straight non-circular bevel gears and virtual non-circular cylindrical gears. LIN et al [15, 16] investigated the tooth profile generating method using the tooth profile of a straight non-circular bevel gear. Thus, since they have not been adequately studied in previous publications, spiral non-circular bevel gears were the object suitable longitudinal curve. When constructed with a circular arc-shaped generating cutter, the longitudinal curve of a face-milling spiral bevel gear is an arc-circle [17–20]. Gears generated with this type of cutter are widely used for mechanical transmission purposes due to their high load carrying capacity, fine dynamic performance, and perfect crafting [21–23]. Thus, spiral non-circular bevel gears with arc-circle longitudinal curves were selected for the purposes of this study.

Spiral non-circular bevel gears, also known as face-milling spiral non-circular bevel gears, are constructed by combining the design principles of non-circular bevel gears and the manufacturing principles of spiral bevel gear. Spiral non-circular bevel gears have many advantages compared to straight non-circular bevel gear, including a high contact ratio, high intensity, good dynamic performance, and an adjustable contact region. Most importantly, this gear type can be fabricated on a 6-axis spiral bevel gear cutting machine, facilitating the application of non-circular bevel gears to the manufacturing industry.

The works conducted in designing the spiral non-circular bevel gear are detailed as follows: First, the face-milling principle was used to generate a spiral non-circular bevel gear. Next, a mathematical model of the spiral non-circular bevel gear, including the tooth profile equation of the flat-top generator, the tooth spiral equation, the pressure angle correction of the cutter, and the enveloping and meshing equations of the tooth profile, was established. Then, the geometric design process was described using a pair of spiral non-circular bevel gears with 2-order sinusoidal gear ratio functions.

Finally, the instantaneous tooth contact area and gear ratio of the designed gear were obtained through transient structural analysis.

## 2 Generating principles of spiral non-circular bevel gear

Non-circular bevel gearing consists of the pure rotation of a drive pitch cone and the driven pitch cone [24] during the driving process. As shown in Figure 1, the generating plane, pitch cone of a drive gear, and pitch cone of a driven gear are all tangent to the contact line ( $OP$ ).

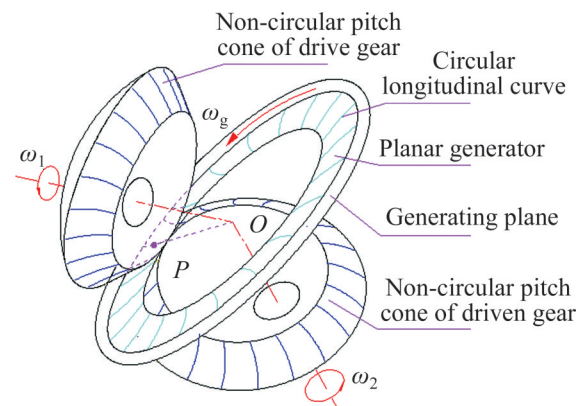


**Figure 1** Generating principle of spiral non-circular bevel gear

Both the drive cone and driven cone rotate along their own axes at a rate of  $\omega$  and  $\omega_2$ , respectively. The generator rotates on the generating plane at a rate of  $\omega_g$ . In this way, the tooth profiles of both drive gear and the driven gear can be generated using the tooth profile of the planar generator [25], all of which satisfy the conjugate meshing condition [26]. Thus, while straight non-circular bevel gears are generated with straight tooth line generators, spiral non-circular bevel gears are generated with arc tooth line generators.

The cutting method for spiral non-circular bevel gears is similar to that of spiral bevel gears. As shown in Figure 2, a head cutter is placed on the generating plane, and the blade of the cutter generates the tooth profile of the spiral non-circular bevel gear. However, a theoretical error exists in that, in this cutting method, the pitch cone of the flat top generator has an approximately  $90^\circ$  pitch angle rather than being a plane (the face cone of the generator is a plane).

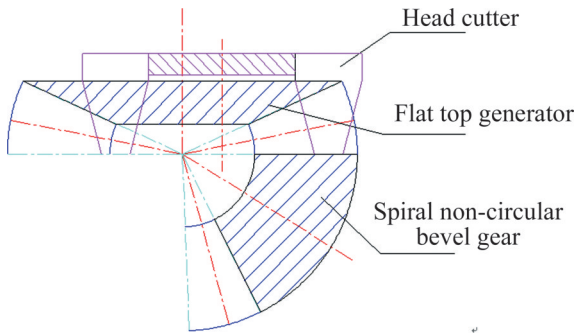


Figure 2 Spiral non-circular bevel gear cutting principles

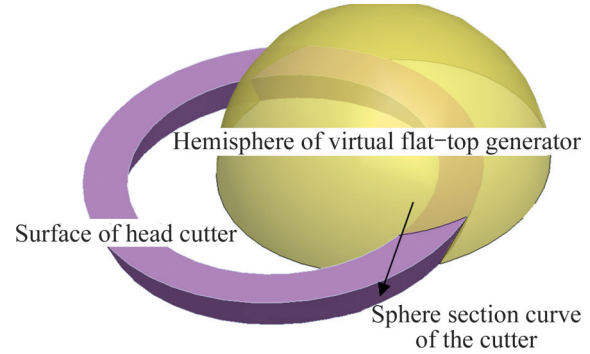


Figure 3 Tooth profile of a virtual flat-top generator

### 3 Mathematical models for spiral non-circular bevel gear

#### 3.1 Tooth profile of flat-top generator

In general, the tooth profile (normal section) of a head cutter is an involute rack. In order to ensure that both sides of a generated gear have the same pressure angle, the convex and concave pressure angles of the cutter,  $\alpha_1$  and  $\alpha_2$ , respectively, were not equal. The theoretical equation of the tooth profile is:

$$\begin{cases} y_v(l) = \begin{cases} -\frac{1}{\tan\alpha_1} \cdot (l + W), & l < -W \\ 0, & -W \leq l < W \\ \frac{1}{\tan\alpha_2} \cdot (l - W), & W \leq l \end{cases} \\ x_v(l) = l \end{cases} \quad (1)$$

where  $W$  is the point width of the cutter blade and  $l$  is the tooth profile variable [27]. After deriving with respect to parameter  $l$ , the equation becomes:

$$\begin{cases} y_v'(l) = \begin{cases} -\frac{1}{\tan\alpha_1}, & l < -W \\ 0, & -W \leq l < W \\ \frac{1}{\tan\alpha_2}, & W \leq l \end{cases} \\ x_v'(l) = 1 \end{cases} \quad (2)$$

According to meshing theory [28], the tooth profile of a virtual flat-top generator is a spherical curve. Thus, in theory, the tooth profile does not lie on the normal section plane of the cutter, but on the spherical curve of the virtual flat-top generator, as depicted in Figure 3.

Figure 4 shows the geometrical relationship

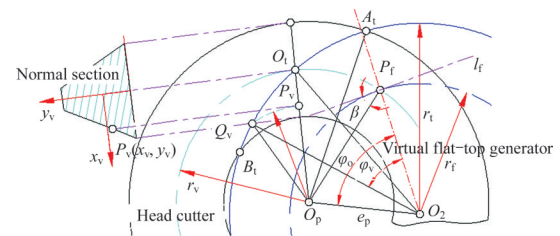


Figure 4 Geometrical relationship between a cutter and virtual flat-top generator

between a cutter and a virtual flat-top generator on a generating plane, or the mapping of the cutter's normal section in the  $x_v$  direction.  $O_p$  and  $O_2$  are the rotary centers of the cutter and flap-top generator, respectively. In addition,  $\overline{O_p O_2} = e_p$  represents distance of the cutter center to the machine center;  $r_v$  represents the mean radius of the cutter;  $r_{vd}$  and  $r_{vx}$  represent the outer radius and inner radius of the cutter respectively. They can be calculated as follows:

$$\begin{cases} r_{vd} = W + h_f \tan\alpha_2 + r_v \\ r_{vx} = -W - h_f \tan\alpha_1 + r_v \end{cases} \quad (3)$$

where  $r_f$  is the mean pitch radius, or mean cone distance, of the generated gear. If  $P_f$  is the intersection of the mean pitch radius ( $r_f$ ) and the cutter radius ( $r_v$ ), and  $O_2 P_f$  is defined as the initial line, then the polar angle of point  $P_f$  is equal to zero. Assume that  $\phi_0$  is the polar angle of point  $O_p$ . Then, according to the law of cosines

$$\phi_0 = \angle P_f O_2 O_p = \arccos\left(\frac{r_f^2 + e_p^2 - r_v^2}{2r_f e_p}\right) \quad (4)$$

where  $l_f$  is the tangent of the mean pitch circle at point  $P_f$ , and the angle to line  $\overline{P_f O_p}$  is the mean spiral angle ( $\beta_f$ ) of the spiral non-circular bevel gear,

which can be calculated as

$$\beta_f = \pi/2 - \angle O_2 P_f O_p = \frac{\pi}{2} - \arccos\left(\frac{r_f^2 + r_v^2 - e_p^2}{2r_f r_v}\right) \quad (5)$$

where  $r_t$  is the spherical radius of the flap-top generator, and  $A_t$ ,  $B_t$  and  $O_t$  are the points of intersection with the cutter radius, inner cutter radius, respectively. Thus,

$$\begin{cases} \angle O_t O_p O_2 = \arccos\left(\frac{r_v^2 + e_p^2 - r_t^2}{2r_v e_p}\right) \\ \angle P_f O_p O_2 = \arccos\left(\frac{r_v^2 + e_p^2 - r_f^2}{2r_v e_p}\right) \end{cases} \quad (6)$$

and the arc length of  $\widehat{O_t P_f}$  is equal to

$$\begin{aligned} L_v &= r_v(\angle O_t O_p O_2 - \angle P_f O_p O_2) \\ &= r_v \arccos\left(\frac{r_v^2 + e_p^2 - r_t^2}{2r_v e_p}\right) - \\ &\quad r_v \arccos\left(\frac{r_v^2 + e_p^2 - r_f^2}{2r_v e_p}\right) \end{aligned} \quad (7)$$

Similarly, the arc length of  $\widehat{A_t B_t}$  is equal to

$$\begin{aligned} L_t &= r_t(\angle A_t O_2 O_p - \angle B_t O_2 O_p) \\ &= r_t \arccos\left(\frac{r_t^2 + e_p^2 - r_{vd}^2}{2r_t e_p}\right) - \\ &\quad r_t \arccos\left(\frac{r_t^2 + e_p^2 - r_{vx}^2}{2r_t e_p}\right) \end{aligned} \quad (8)$$

Furthermore, if  $r_t = r_p$ , then the arc length of the mean pitch sphere is

$$\begin{aligned} L_f &= r_f \arccos\left(\frac{r_f^2 + e_p^2 - r_{vd}^2}{2r_f e_p}\right) - \\ &\quad r_f \arccos\left(\frac{r_f^2 + e_p^2 - r_{vx}^2}{2r_f e_p}\right) \end{aligned} \quad (9)$$

Thus, the module of the flat-top generator is equal to

$$\begin{aligned} m_f &= \frac{L_f}{\pi} = \frac{r_f}{\pi} \arccos\left(\frac{r_f^2 + e_p^2 - r_{vd}^2}{2r_f e_p}\right) - \\ &\quad \frac{r_f}{\pi} \arccos\left(\frac{r_f^2 + e_p^2 - r_{vx}^2}{2r_f e_p}\right) \end{aligned} \quad (10)$$

As shown in Figure 4, the normal section of the cutter lies on line  $\widehat{O_p O_t}$ , while the tooth profile of the flat-top generator lies on arc  $\widehat{A_t B_t}$ . Assume that

$P(x_v, y_v)$  is a point on the normal profile of the cutter with corresponding point ( $Q_v$ ) on arc  $\widehat{A_t B_t}$ . Thus,

$$\overline{O_p Q_v} = \overline{O_p P_v} = r_v - x_v \quad (11)$$

In terms of the law of cosines,

$$\angle O_v O_2 O_p = \arccos\left(\frac{r_t^2 + e_p^2 - (r_v - x_v)^2}{2r_t e_p}\right) \quad (12)$$

If the polar angle of point  $Q_v$  is  $\varphi_v$ , then

$$\begin{aligned} \varphi_v &= \angle Q_v O_2 P_f = \varphi_0 - \angle O_v O_2 O_p \\ &= \arccos\left(\frac{r_f^2 + e_p^2 - r_v^2}{2r_f e_p}\right) - \\ &\quad \arccos\left(\frac{r_t^2 + e_p^2 - (r_v - x_v)^2}{2r_t e_p}\right) \end{aligned} \quad (13)$$

And the spiral angle of  $Q_v$  is equal to

$$\begin{aligned} \beta_t &= \pi/2 - \angle O_2 Q_v O_p \\ &= \frac{\pi}{2} - \arccos\left(\frac{r_f^2 + (r_v - x_v)^2 - e_p^2}{2r_f (r_v - x_v)}\right) \end{aligned} \quad (14)$$

One of the polar angles of the flat-top generators is defined in Eq. (13). As shown in Figure 5, the other polar angle of point  $Q_v$  is  $\delta_v$ , which can be calculated as:

$$\delta_v = \arcsin\left(\frac{y_v + h_f}{r_t}\right) \quad (15)$$

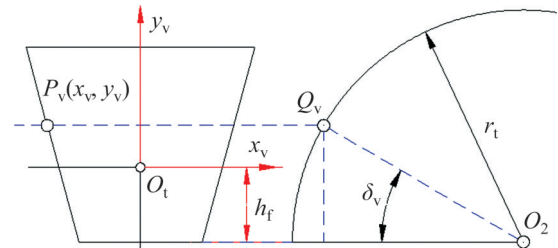


**Figure 5** Geometrical relationship of cutter and virtual flat-top generator

According to the discussion above, the spherical coordinates of point  $Q_v$  are  $(\varphi_v, \delta_v)$ , and its Cartesian form, for coordinate transformation, is

$$r_2 = \begin{bmatrix} r_t \sin\delta_v \cos\varphi_v \\ r_t \sin\delta_v \sin\varphi_v \\ r_t \cos\delta_v \\ 1 \end{bmatrix} \quad (16)$$

### 3.2 Basic cones of non-circular bevel gears

Figure 6 displays the three basic cones of a

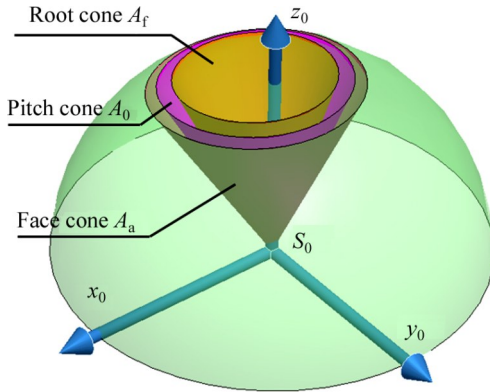


**Figure 6** Basic cones of non-circular bevel gears

non-circular bevel gear: the pitch cone ( $A_0$ ), root cone ( $A_f$ ), and face cone ( $A_a$ ). The reference frame,  $S_0(O_0 - x_0, y_0, z_0)$ , is fixed at the gear center, and the pitch curve of the non-circular bevel gear can be represented by the vector function  $r_{A_0}(\varphi_1, R)$  as [29].

$$r_{A_0}(\varphi_1, R) = [R \sin \delta_0 \cos \varphi_0 \quad R \sin \delta_0 \sin \varphi_0 \quad R \cos \delta_0 \quad 1]^T \quad (17)$$

where  $R$  is the radius of the pitch cone;  $\varphi_0$  is the rotating angle of the non-circular bevel gear; and  $\delta_0$  is the pitch angle. For a pair of non-circular bevel gears;  $\varphi_1$  and  $\varphi_2$  can be defined as the rotating angles of the drive gear and driven gear, respectively;  $\delta_1$  and  $\delta_2$  can be defined as the pitch angles of drive gear and driven gear, respectively. In general, the gear ratio can be represented by the  $\varphi_1$  function, namely,  $i_{12} = i_{12}(\varphi_1)$ . Thus,  $\varphi_2 = \int_0^{\varphi_1} \frac{1}{i_{12}(\varphi)} d\varphi$ . If the shaft angle is equal to  $90^\circ$ , the pitch angle can be calculated as:

$$\begin{cases} \delta_1 = \text{arccot} [i_{12}(\varphi_1)] \\ \delta_2 = \text{arctan} [i_{12}(\varphi_1)] \end{cases} \quad (18)$$

By substituting  $R = r_f$  in Eq. (17), the mean pitch curve of the spiral non-circular bevel gear can be obtained. Its arc-length [30], can be obtained by

$$\begin{aligned} L_p &= \int_0^{2\pi} \left\{ \left[ \frac{d(r_f \sin \delta_0 \cos \varphi)}{d\varphi} \right]^2 + \right. \\ &\quad \left. \left[ \frac{d(r_f \sin \delta_0 \sin \varphi)}{d\varphi} \right]^2 + \left[ \frac{d(r_f \cos \delta_0)}{d\varphi} \right]^2 \right\}^{1/2} d\varphi \\ &= r_f \int_0^{2\pi} \sqrt{\delta_0'^2 + \sin^2 \delta_0} d\varphi \end{aligned} \quad (19)$$

Assume that the tooth number of the generated gear is  $z$ . Then, the mean module, or module on the mean pitch curve, is equal to

$$m_F = \frac{L_p}{\pi z} = \frac{r_f \int_0^{2\pi} \sqrt{\delta_0'^2 + \sin^2 \delta_0} d\varphi}{\pi z} \quad (20)$$

In order to ensure that the generated drive and driven gears satisfy the conjugate meshing condition for the same generator, the mean module must be equal to the flat-top generator module.

$$m_F = m_f \quad (21)$$

In general, the root cone and face cone can be different in different tooth systems. In this paper, however, these cones were defined as cones with an angle constant to the pitch cone. Assume that  $P_0(\delta_0, \varphi_0, R)$  is a point on the pitch cone. Then,  $t_1$  is the tangent vector of pitch cone  $A_0$  in the circumferential direction at point  $P_0$ , which can be calculated as [31].

$$\begin{aligned} t_1 &= \left[ \frac{d(R \sin \delta_0 \cos \varphi_0)}{d\varphi_0} \quad \frac{d(R \sin \delta_0 \sin \varphi_0)}{d\varphi_0} \quad \frac{d(R \cos \delta_0)}{d\varphi_0} \right]^T \\ &= R \begin{bmatrix} \delta_0' \cos \delta_0 \cos \varphi_0 - \sin \delta_0 \sin \varphi_0 \\ \delta_0' \cos \delta_0 \sin \varphi_0 + \sin \delta_0 \cos \varphi_0 \\ -\delta_0' \sin \delta_0 \end{bmatrix} \end{aligned} \quad (22)$$

Then the unit tangent vector is equal to

$$t_{1u} = \frac{t_1}{|t_1|} = \begin{bmatrix} \frac{\delta_0' \cos \delta_0 \cos \varphi_0 - \sin \delta_0 \sin \varphi_0}{\sqrt{\delta_0'^2 + \sin^2 \delta_0}} \\ \frac{\delta_0' \cos \delta_0 \sin \varphi_0 + \sin \delta_0 \cos \varphi_0}{\sqrt{\delta_0'^2 + \sin^2 \delta_0}} \\ \frac{-\delta_0' \sin \delta_0}{\sqrt{\delta_0'^2 + \sin^2 \delta_0}} \end{bmatrix} \quad (23)$$

The tangent vector of the pitch cone ( $A_0$ ) in the radial direction at point  $P_0$  is equal to

$$\begin{aligned} t_2 &= \left[ \frac{d(R \sin \delta_0 \cos \varphi_0)}{dR} \quad \frac{d(R \sin \delta_0 \sin \varphi_0)}{dR} \quad \frac{d(R \cos \delta_0)}{dR} \right]^T \\ &= [\sin \delta_1 \cos \varphi_0 \quad \sin \delta_1 \sin \varphi_0 \quad \cos \delta_1]^T \end{aligned} \quad (24)$$

And its corresponding unit vector is equal to

$$t_{2u} = t_2 = [\sin \delta_1 \cos \varphi_0 \quad \sin \delta_1 \sin \varphi_0 \quad \cos \delta_1]^T \quad (25)$$

The unit normal vector of the pitch cone at point  $P_0$  can be calculated using the cross product of the two tangent unit vectors as follows.

$$\mathbf{n}_{1u} = \mathbf{t}_{1u} \times \mathbf{t}_{2u}$$

$$= \begin{bmatrix} \frac{\cos\delta_0 \sin\delta_0 \cos\varphi_0 - \delta'_0 \cos^2\delta_0 \sin\varphi_0 + \delta'_0 \sin^2\delta_0 \sin\varphi_0}{\sqrt{\delta_0'^2 + \sin^2(\delta_0)}} \\ \frac{\cos\delta_0 \sin\delta_0 \sin\varphi_0 - \delta'_0 \cos^2\delta_0 \cos\varphi_0 - \delta'_0 \sin^2\delta_0 \cos\varphi_0}{\sqrt{\delta_0'^2 + \sin^2(\delta_0)}} \\ \frac{2\delta'_0 \sin\delta_0 \cos\delta_0 \sin\varphi_0 \cos\varphi_0 - \sin^2\delta_0}{\sqrt{\delta_0'^2 + \sin^2\delta_0}} \end{bmatrix} \quad (26)$$

The root cone and face cone can be represented in terms of the unit normal vector by

$$\begin{cases} \mathbf{r}_{Af}(\varphi_0, R) = \mathbf{r}_{A0}(\varphi_0, R) - \frac{h_a}{r_f} R \mathbf{n}_{1u}(\varphi_0, R) \\ \mathbf{r}_{Aa}(\varphi_0, R) = \mathbf{r}_{A0}(\varphi_0, R) + \frac{h_f}{r_f} R \mathbf{n}_{1u}(\varphi_0, R) \end{cases} \quad (27)$$

where  $h_a$  and  $h_f$  are the addenduma and dedendums of the teeth.

### 3.3 Applied coordinate system

Theoretically, based on the generating principles shown in Figures 1 and 2 and the methods presented in Ref. (16)–(18), the kinematic geometrical relationship of generating spiral non-circular bevel gear can be established. However, due to the complexity of the method above, a new method based on the normal vector of the pitch cone was proposed. The proposed method was more concise since it involved vector algebra rather than complex spatial angle and position calculations.

As shown in Figure 7, the generated gear is fixed on the ground, the coordinate system  $S_0(O_0 - x_0 y_0 z_0)$  is fixed on generated gear,  $A_p$  is the face cone of the flat-top generator (a plane),  $O_f P_f$  is the tangent line of root cone  $A_f$  and the plane  $A_p$ , and  $P_f$  is the contact point of plane  $A_p$  and root cone  $A_f$  on the mean radius ( $r_f$ ). Substitute  $R = r_f$  into Eq. (24), there will be

$$\mathbf{r}_{Pf}(\varphi_0) = \mathbf{r}_{A0}(\varphi_0, r_f) + h_f \mathbf{n}_{1u} \quad (28)$$

In terms of Eq. (27), the unit tangent vector of the root cone in the circumferential direction ( $\mathbf{t}_{3u}$ ) is equal to that of the pitch cone ( $\mathbf{t}_{1u}$ ), namely,

$$\mathbf{t}_{3u} = \mathbf{t}_{1u} \quad (29)$$

And the unit tangent vector of the root cone ( $A_f$ ) in the radial direction ( $\mathbf{t}_{2u}$ ) can be calculated as

$$\mathbf{t}_{2u} = \mathbf{M}_{f0} \mathbf{t}_{2u} \quad (30)$$

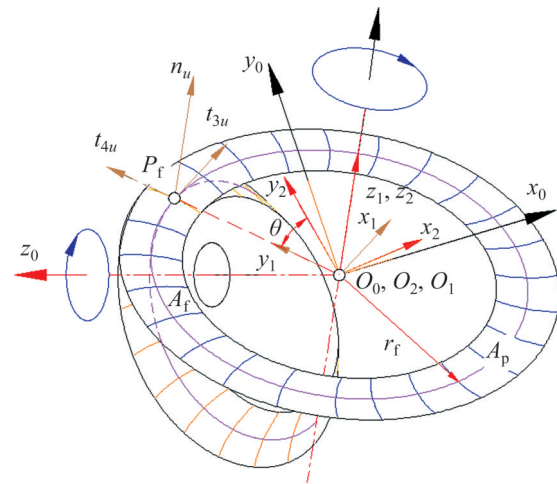


Figure 7 Geometrical relationship of the generating spiral non-circular bevel gear

where

$$\mathbf{M}_{f0} = \begin{bmatrix} 1 & 0 & 0 \\ 0 & \cos\delta_f & \sin\delta_f \\ 0 & -\sin\delta_f & \cos\delta_f \end{bmatrix}$$

Thus, the unit normal vector of the root cone ( $A_f$ ) at point  $P_f$  can be measured by the cross product of the two tangent unit vectors as

$$\mathbf{n}_{3u} = \mathbf{t}_{3u} \times \mathbf{t}_{4u} \quad (31)$$

A mobile Cartesian coordinate system  $S_1(O_1 - x_1 y_1 z_1)$  was established at point  $O_0$  based on the directions of the above vectors. The  $x_1$ -axis was in the direction of  $\mathbf{n}_{3u}$ , the  $y_1$ -axis was in the direction of  $\mathbf{t}_{3u}$ , and the  $z_1$ -axis was in the direction of  $\mathbf{t}_{4u}$ .

The base vector of coordinate system  $S_0$  is

$$\begin{cases} \mathbf{i}_0 = [1 & 0 & 0]^T \\ \mathbf{j}_0 = [0 & 1 & 0]^T \\ \mathbf{k}_0 = [0 & 0 & 1]^T \end{cases} \quad (32)$$

And the base vector of coordinate system  $S_1$  is

$$\begin{cases} \mathbf{i}_1 = \mathbf{n}_{3u} \\ \mathbf{j}_1 = \mathbf{t}_{3u} \\ \mathbf{k}_1 = \mathbf{t}_{4u} \end{cases} \quad (33)$$

The relationship between the mobile coordinate system ( $S_1$ ) and the ground coordinate system ( $S_0$ ) can be obtained using the vector transformation method [32],

$$\begin{aligned}
 M_{01} &= \begin{bmatrix} \mathbf{i}_0 \times \mathbf{i}_1 & \mathbf{i}_0 \times \mathbf{j}_1 & \mathbf{i}_0 \times \mathbf{k}_1 & 0 \\ \mathbf{j}_0 \times \mathbf{i}_1 & \mathbf{j}_0 \times \mathbf{j}_1 & \mathbf{j}_0 \times \mathbf{k}_1 & 0 \\ \mathbf{k}_0 \times \mathbf{i}_1 & \mathbf{k}_0 \times \mathbf{j}_1 & \mathbf{k}_0 \times \mathbf{k}_1 & 0 \\ 0 & 0 & 0 & 1 \end{bmatrix} \\
 &= \begin{bmatrix} \mathbf{n}_{3ux} & \mathbf{t}_{3ux} & \mathbf{t}_{4ux} & 0 \\ \mathbf{n}_{3uy} & \mathbf{t}_{3uy} & \mathbf{t}_{4uy} & 0 \\ \mathbf{n}_{3uz} & \mathbf{t}_{3uz} & \mathbf{t}_{4uz} & 0 \\ 0 & 0 & 0 & 1 \end{bmatrix} \tag{34}
 \end{aligned}$$

where  $\mathbf{n}_{3ux}$ ,  $\mathbf{n}_{3uy}$  and  $\mathbf{n}_{3uz}$  are the vector component of the normal vector ( $\mathbf{n}_{3u}$ ) in three axes;  $\mathbf{t}_{3ux}$ ,  $\mathbf{t}_{3uy}$  and  $\mathbf{t}_{3uz}$  are the vector components of the tangent vector ( $\mathbf{t}_{3u}$ ); and  $\mathbf{t}_{4ux}$ ,  $\mathbf{t}_{4uy}$  and  $\mathbf{t}_{4uz}$  are the vector components of the tangent vector ( $\mathbf{t}_{4u}$ ).

Assume that the mobile coordinate system,  $S_2(O_2 - x_2y_2z_2)$ , is fixed on the generator, and its angle to the coordinate system ( $S_1$ ) is  $\theta_p$ . In order to satisfy the conjugate meshing requirement, a pure rolling relationship should exist between the pitch cones of the gear and generator such that

$$\begin{aligned}
 \theta_p &= \left\{ \int_0^{\varphi_0} \left[ \left( \frac{d(R \sin \delta_0 \cos \varphi)}{d\varphi} \right)^2 + \left( \frac{d(R \sin \delta_0 \sin \varphi)}{d\varphi} \right)^2 + \left( \frac{d(R \cos \delta_0)}{d\varphi} \right)^2 \right]^{1/2} d\varphi \right\} / r_f \\
 &= \frac{\int_0^{\varphi_1} r_f \sqrt{\delta_0'^2 + \sin^2 \delta_0} d\varphi}{r_f} \tag{35}
 \end{aligned}$$

In addition, the coordinate relationship between coordinate system  $S_2$  and mobile coordinate system  $S_1$  is as follows:

$$M_{12} = \begin{bmatrix} \cos\theta & \sin\theta & 0 & 0 \\ -\sin\theta & \cos\theta & 0 & 0 \\ 0 & 0 & 1 & 0 \\ 0 & 0 & 0 & 1 \end{bmatrix} \tag{36}$$

Thus, the coordinate transformation relationship between mobile coordinate system  $S_2$  and ground coordinate system  $S_0$  is:

$$\begin{aligned}
 M_{02} &= M_{01} M_{12} \\
 &= \begin{bmatrix} \mathbf{n}_{3ux} \cos\theta_p - \mathbf{t}_{3ux} \sin\theta_p & \mathbf{n}_x \sin\theta_p + \mathbf{t}_{3ux} \cos\theta_p & \mathbf{t}_{4ux} & 0 \\ \mathbf{n}_{3uy} \cos\theta_p - \mathbf{t}_{3uy} \sin\theta_p & \mathbf{n}_y \sin\theta_p + \mathbf{t}_{3uy} \cos\theta_p & \mathbf{t}_{4uy} & 0 \\ \mathbf{n}_{3uz} \cos\theta_p - \mathbf{t}_{3uz} \sin\theta_p & \mathbf{n}_z \sin\theta_p + \mathbf{t}_{3uz} \cos\theta_p & \mathbf{t}_{4uz} & 0 \\ 0 & 0 & 0 & 1 \end{bmatrix} \tag{37}
 \end{aligned}$$

### 3.4 Tooth spiral

As shown in Figure 8,  $O_2P_0$  is the contact line between the generating plane and the pitch cone of the generated gear,  $r_d$  and  $r_x$  are the toe pitch radius and heel pitch radius of the non-circular bevel gear (as well as the toe pitch radius and heel pitch radius of the generating plane), and  $O_xO_d$  is the sectional curve of the cutter between the toe and heel of generating plane. During the generating process, the contact point ( $P_0$ ) moves continuously on the arc ( $O_xO_d$ ), producing a curve ( $C_s$ ) on the pitch cone of the generated gear. This curve ( $C_s$ ) is the tooth spiral of the spiral non-circular bevel gear. Assume that point  $O_t$  is a contact point on arc  $O_xO_d$  and that its corresponding point on the tooth spiral is  $P_t$ .

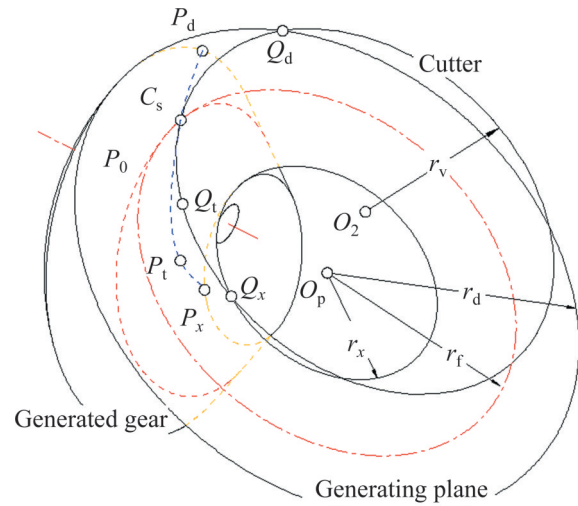


Figure 8 Tooth spiral generating

Then, in terms of Eq. (19), the arc length of curve  $P_0P_t$  is

$$L_c = r_t \int_{\varphi_t}^{\varphi_1} \sqrt{\delta_0'^2 + \sin^2 \delta_0} d\varphi \tag{38}$$

where  $\varphi_t$  is the rotary angle of the generated gear at point  $P_t$ , and  $\varphi_0$  is the rotary angle of the generated gear at point  $P_0$ . According to the pure rolling relationship, the arc length of arc  $P_0O_t$  is equal to curve  $P_0P_t$  in that

$$\overline{P_0O_t} = L_c \tag{39}$$

By substituting Eq. (7) into Eq. (38), the relationship between point  $P_t$  and point  $O_t$  can be represented as

$$r_t \int_{\varphi_f}^{\varphi_t} \sqrt{\delta_0'^2 + \sin^2 \delta_0} d\varphi = r_v \arccos\left(\frac{r_v^2 + e_p^2 - r_t^2}{2r_v e_p}\right) - r_v \arccos\left(\frac{r_v^2 + e_p^2 - r_f^2}{2r_v e_p}\right) \quad (40)$$

Then, by substituting  $r_t = r_x - r_d$  into Eq. (40), the tooth spiral curve ( $C_s$ ) can be obtained.

### 3.5 Pressure angle

According to meshing theory, the normal vector of the generating cutter is equal to that of the generated gear [33]. In addition, in order to ensure equal transmission performance during positive and negative rotation, the convex and concave flanks of a generated gear should, in general, have equal pressure angles [34]. However, according to the generating method above, the normal vectors of the convex and concave sides of a cutter are different. Thus, cutter pressure angle correction was implemented.

As shown in Figure 9, the pressure angles of points  $F_1$  (internal side) and  $F_2$ (external side) were calculated, and their corresponding coordinate values were approximately  $F_1\left(-\frac{\pi m}{4}, 0\right)$  and  $F_2\left(\frac{\pi m}{4}, 0\right)$ , respectively. The normal vectors of the flanks at these points are  $\mathbf{n}_{e1}$  and  $\mathbf{n}_{e2}$ , respectively, and their corresponding projective vectors,  $\mathbf{b}_{e1}$  and  $\mathbf{b}_{e2}$ , can be calculated as

$$\begin{cases} \mathbf{b}_{e1} = |\mathbf{n}_{e1}| \cos(\alpha_1 - \delta_f) = \cos(\alpha_1 - \delta_f) \\ \mathbf{b}_{e2} = |\mathbf{n}_{e2}| \cos(\alpha_2 + \delta_f) = \cos(\alpha_2 + \delta_f) \end{cases} \quad (41)$$

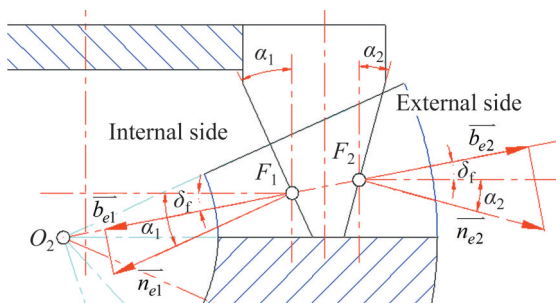


Figure 9 Normal vector of cutter in cutter section plane

Figure 10 shows the normal vector of the cutter in generating plane, where  $\mathbf{c}_{e1}$  and  $\mathbf{c}_{e2}$  are the projective vectors of  $\mathbf{b}_{e1}$  and  $\mathbf{b}_{e2}$  in the tangential direction of the mean pitch circle, namely, the tooth

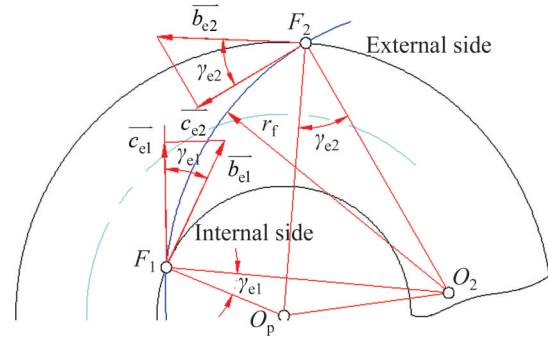


Figure 10 Normal vector of cutter in generating plane

profile vectors, which can be calculated as:

$$\begin{cases} \mathbf{c}_{e1} = \mathbf{b}_{e1} \cos \gamma_1 = \cos \alpha_1 - \delta_f \cos \gamma_1 \\ \mathbf{c}_{e2} = \mathbf{b}_{e2} \cos \gamma_2 = \cos \alpha_2 + \delta_f \cos \gamma_2 \end{cases} \quad (42)$$

where

$$\begin{cases} \gamma_1 = \arccos\left[\frac{r_t^2 + \left(r_v - \frac{\pi m}{4}\right)^2 - e_p^2}{2r_t\left(r_v - \frac{\pi m}{4}\right)}\right] \\ \gamma_2 = \arccos\left[\frac{r_t^2 + \left(r_v + \frac{\pi m}{4}\right)^2 - e_p^2}{2r_t\left(r_v + \frac{\pi m}{4}\right)}\right] \end{cases} \quad (43)$$

in order to ensure that the two sides of the tooth profile have equal pressure angles, such that

$$|\mathbf{c}_{e1}| = |\mathbf{c}_{e2}| \quad (44)$$

The two sides of the cutter can be obtained by substituting Eqs. (41) and (42) into Eq. (43) as follows.

$$\frac{\cos(\alpha_1 - \delta_f)}{\cos(\alpha_2 + \delta_f)} = \frac{r_v - \frac{\pi m}{4}}{r_v + \frac{\pi m}{4}} \cdot \frac{r_t^2 + \left(r_v + \frac{\pi m}{4}\right)^2 - e_p^2}{r_t^2 + \left(r_v - \frac{\pi m}{4}\right)^2 - e_p^2} \quad (45)$$

The method above used to calculate the pressure angle relationships in the cutter is somewhat different from those used in Refs. [30, 31], but, fundamentally, they are the same.

### 3.6 Tooth profile

Using the tooth profile of the flat-top generator obtained in Eq. (16) and the coordinate transformation matrices of the flat-top generator and



generated gear presented in Eq. (37), the envelope equation of the generated gear can be derived by substituting the tooth profile of the generator into the coordinate system of the generated gear as follows.

$$\mathbf{r}_0 = \mathbf{M}_{02}\mathbf{r}_2 \quad (46)$$

The tangent vectors of the generator's tooth profile in two different directions are

$$\left\{ \begin{aligned} \mathbf{t}_1 &= \begin{bmatrix} \frac{dr_t \sin\delta_v \cos\varphi_v}{dl} \\ \frac{dr_t \sin\delta_v \sin\varphi_v}{dl} \\ \frac{r_t \cos\delta_v}{dl} \end{bmatrix} \\ &= r_t \begin{bmatrix} \varphi'_v \cos\delta_v \cos\varphi_v - \delta'_v \sin\delta_v \sin\varphi_v \\ -\varphi'_v \cos\delta_v \sin\varphi_v - \delta'_v \sin\delta_v \cos\varphi_v \\ \delta'_v \cos\delta_v \end{bmatrix} \\ \mathbf{t}_r &= \begin{bmatrix} \frac{dr_t \sin\delta_v \cos\varphi_v}{dr_t} \\ \frac{dr_t \sin\delta_v \sin\varphi_v}{dr_t} \\ \frac{r_t \cos\delta_v}{dr_t} \end{bmatrix} = \begin{bmatrix} \sin\delta_v \cos\varphi_v \\ \sin\delta_v \sin\varphi_v \\ \cos\delta_v \end{bmatrix} \end{aligned} \right. \quad (47)$$

where

$$\left\{ \begin{aligned} \varphi'_v &= \frac{d\varphi_v}{dl} = \frac{x'_v(r_v - x_v)}{r_f e_p \sqrt{1 - \frac{r_f^2 + e_p^2 - (r_v - x_v)^2}{4r_f^2 e_p^2}}} \\ \delta'_v &= \frac{d\delta_v}{dl} = \frac{1}{r_t \sqrt{1 - \frac{y_v^2}{r_t^2}}} \end{aligned} \right. \quad (48)$$

Thus, the normal vector of the generator's tooth profile is:

$$\mathbf{n}_r = \mathbf{t}_1 \times \mathbf{t}_r \quad (49)$$

In general, the relative velocity between the generator and generated gear is calculated in terms of the kinematic relationships between their different coordinate systems, and the geometric relationship between the generating plane and generated gear is based on the normal vector of the pitch cone. Due to the relative positional relationship between the generator and generated gear presented in Eq. (45), the relative velocity can be obtained by deriving Eq. (45) with respect to time [35] as follows:

$$\begin{aligned} \mathbf{v}_c &= \frac{d\mathbf{r}_0}{dt} = \frac{d\mathbf{r}_0}{d\varphi_0} \frac{d\varphi_0}{dt} = \omega_1 \frac{d\mathbf{r}_0}{d\varphi_0} = \omega_1 \frac{d(\mathbf{M}_{02}\mathbf{r}_2)}{d\varphi_0} \\ &= \omega_1 \frac{d\mathbf{M}_{02}}{d\varphi_0} \mathbf{r}_2 \end{aligned} \quad (50)$$

where  $\omega_1$  is the relative velocity between the mobile coordinate system  $(O_1x_1y_1z_1)$  and ground coordinate system  $(O_0x_0y_0z_0)$ , which is constant, and  $\frac{d\mathbf{M}_{02}}{d\varphi_0}$  is the derivative of each component in the coordinate transformation matrix  $(\mathbf{M}_{02})$  with respect to  $\varphi_0$ .

According to the meshing principle, the tooth profile of a generated gear must satisfy the following equation:

$$\mathbf{n}_r \cdot \mathbf{v}_c = 0 = \mathbf{n}_r \left( \frac{d\mathbf{M}_{02}}{d\varphi_1} \mathbf{r}_2 \right) \quad (51)$$

Thus, the tooth profile of a generated spiral non-circular bevel gear can be obtained by solving the meshing and envelope equations (Eq. (49) and Eq. (45)) described above.

#### 4 Geometric designs of spiral non-circular bevel gear

The geometric design of spiral non-circular bevel gears can be performed based on the mathematical model above. In this paper, a pair of spiral non-circular bevel gears with 2-order sinusoidal gear ratio function was used as an example. The drive gear (pinion) and driven gear (gear) of the spiral non-circular bevel gears used in this paper had the same generator (cutter) and date of design. The head cutter and machine-tools setting are shown in Tables 1–3.

In terms of the basic kinematic relationships of non-circular gears [36], the rotation angle of a driven gear is

$$\varphi_2(\varphi_1) = \int_0^{\varphi_1} \frac{1}{2.154 + 0.8\cos\varphi_1} d\varphi \quad (52)$$

Thus,  $\varphi_2(2\pi) = \pi$ , and, when the drive gear completes a cycle, the driven gear completes half of a cycle. The tooth number of the driven gear is

$$z_2 = 2z_1 = 20$$

Based on Eq. (18), the pitch cone angles of the drive and driven gears are, respectively, equal to

**Table 1** Design dates of spiral non-circular bevel gears

Parameter	Module/mm	Shaft angle/(°)	Gear ratio function	Face wide/mm	Mean cone distance/mm	Number of teeth
Drive gear	3	90	—	20	50	10
Driven gear	3	90	—	20	50	20
Parameter	Mean spiral angle/(°)	Addendum/mm	Dedendum/mm	Clearance/mm	Hand of spiral	
Drive gear	35	3	3.75	0.75	LH	
Driven gear	35	3	3.75	0.75	RH	

**Table 2** Date of head cutter

Radius of cutter, $r_c$ /mm	Point width/mm	Pressure angle, convex/(°)	Pressure angle, concave/(°)	Tip fillet radius/mm
38.1 (1.5int)	1.6	24.5	19.5	0

**Table 3** Machine-tool settings

Gear	Machine center to back/mm	Sliding base/mm	Blank offset/mm	Cradle angle of cutter/(°)	Radial distance/mm	Machine root angle
Drive gear	Concave	0	0.21	0	62.364	35.162
	Convex	0	0.21	0	61.722	34.963
Driven gear	0.25	0	0	55.283	35.061	Varying

$$\begin{cases} \delta_1 = \text{arccot}(0.8\cos\varphi_1 + 2.154) \\ \delta_2 = \text{arctan}(0.8\cos\varphi_1 + 2.154) \end{cases} \quad (53)$$

Based on Eq. (17), the pitch cones of the drive and driven gears are, respectively, equal to (shown in Figure 11)

$$A_1(R, \varphi_1) = \begin{bmatrix} R \sin [\text{arccot}(0.8\cos\varphi_1 + 2.154)] \cos\varphi_1 \\ R \sin [\text{arccot}(0.8\cos\varphi_1 + 2.154)] \sin\varphi_1 \\ R \cos [\text{arccot}(0.8\cos\varphi_1 + 2.154)] \\ 1 \end{bmatrix} \quad (54)$$

According to Eq. (19), the arc length of the mean pitch curve is  $L_p = 115.274$ .

Based on Eq. (5), the center distance of the cutter is  $e_p = 37.197$ .

In addition, the tooth spirals of the drive and driven gears, as shown in Figure 11, can be determined by substituting  $\varphi_i = \frac{2\pi}{z_1}i$  ( $i=0, 1, \dots, z_1$ ) into Eq. (40).

According to Eq. (20), the mean module is equal to

$$m_F = \frac{L_p}{\pi z_1} = 3.67 \quad (55)$$

Furthermore, the module of the flat-top generator ( $m_p$ ) can be calculated with Eq. (10). Then, in combination with Eq. (21), the module of

the cutter can be solved as  $m = 3$ . Thus, the tooth profile of the flat-top generator (shown in Figure 12) can be obtained with Eq. (16).

The tooth envelope surfaces generated by the flat-top generators of the drive and driven gears can be obtained using Eq. (45). Figure 13 displays the

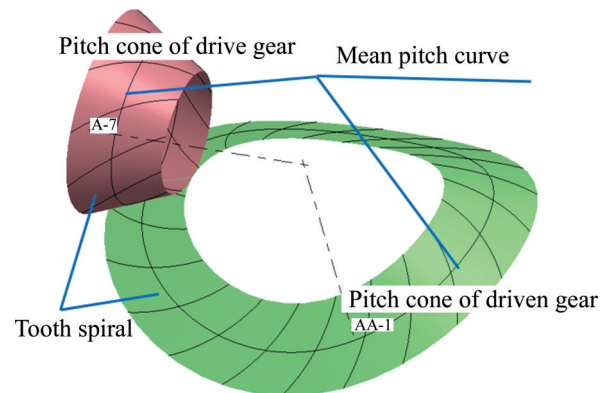


**Figure 11** Pitch cones of drive gear and driven gear

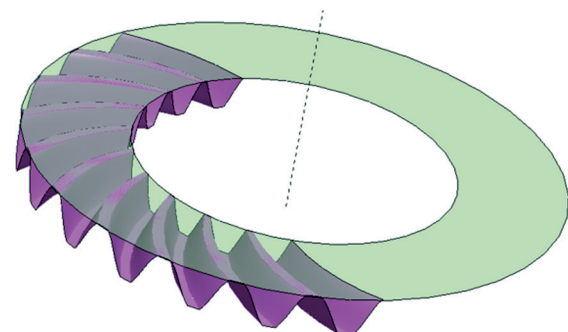


**Figure 12** Tooth profile of flat-top generator

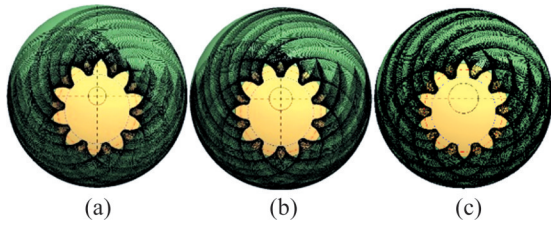


**Figure 13** Tooth envelope curves of drive gears in different spheres: (a)  $r_t = r_d$ ; (b)  $r_t = r_p$ ; (c)  $r_t = r_x$

envelope curves of the drive gears in different spheres.

By combining the meshing equation (Eq. (49)) and envelope equation (Eq. (45)), the boundary of the tooth envelope curve, or the tooth profile surface of the generated gear, can be solved. Figure 14 displays 3D models of the drive and driven gears, and Figure 15 displays the virtual assembly of these two meshing gears.

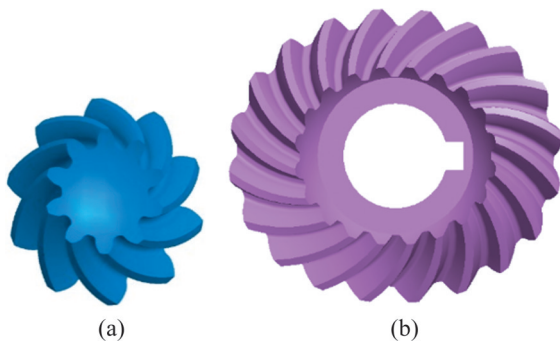


**Figure 14** 3D models of drive and driven gears: (a) Drive gear; (b) Driven gear

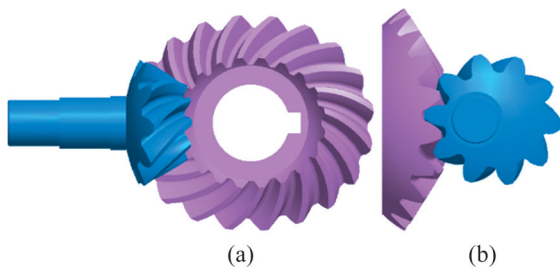


**Figure 15** Virtual assembly of contact gears: (a) Front view; (b) Left view

### 5 Tooth contact analysis using finite element method

Since the tooth profiles of non-circular gears are different for each tooth, the tooth contact forces and contact areas of each tooth are also different. Thus, a static contact analysis would not be feasible

for these purposes. Rather, a transient structural analysis was conducted in order to determine the evolution of the contact area during the meshing cycle.

Finite element models of all of the teeth for both the drive and the driven gears were used to maintain the difference between the boundary conditions and the tooth loaded areas and to study the evolution of the contact area on the flanks of the drive and driven gears.

However, since the transient structural analysis was time-consuming and computationally expensive, a maximum level for the simplified finite models was established. First, a non-circular cone was constructed by substituting  $h = -1.2h_f$  into Eq. (27). Then, the geometrical entity was removed from within the normal cone surface. Finally, the left geometry entity was meshed with SOLID187 elements, as shown in Figure 16. SOLID187 elements are high-order, 3-D, 10-node elements with quadratic displacement behaviors that are well-suited to large deflection and large strain deflection. The tooth flanks of drive gears are considered to be master surfaces (CONTACT174 elements) and the tooth flanks of driven gears are considered to be slave surfaces (TARGE170 elements). The total amounts of the different element types used in the finite model are shown in Table 4.

Steel with a elastic module of 210 GPa and a

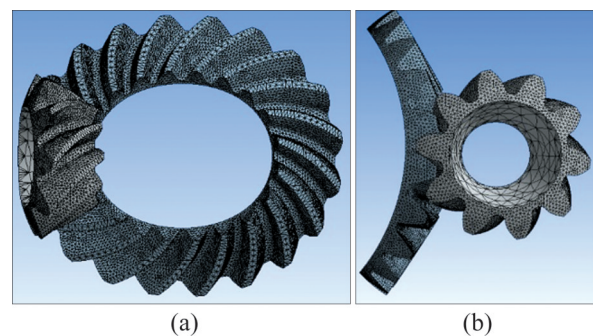


**Figure 16** Finite element models of contact gears: (a) Front view; (b) Left view

**Table 4** Elements of finite model

Gear	Element type	Number
Drive gear	SOLID187	17110
	CONTACT174	11657
Driven gear	SOLID187	25447
	TARGE170	11657

Poisson’s ratio of 0.3 was used for the analysis. The concave side of the drive tooth surface and the convex side of the driven tooth surface were considered to be the drive and driven surfaces, respectively. In addition, an angular velocity of 6.28 rad/s in the anti-clockwise direction and a torque of 10 N·m in the clockwise direction were implemented in the drive and driven gears, respectively. In order to make the drive gear complete a cycle and then detect the corresponding contact area on each tooth flank, the analysis time was established to be equal to 1 s.

As shown in Figure 17 (blue curve), the angular velocity of driven gear was obtained. The theoretical angular velocity of the driven gear ( $\omega_2$ ) was also obtained using the gear ratio listed in Table 1, as shown in Figure 17 (red curve).

$$\omega_2 = \omega_1/i_{12}(\omega_1 t) = \frac{\omega_1}{2.154 + 0.8\cos(\omega_1 t)} \quad (56)$$

By comparing the analyzed curve (blue) with the theoretical curve (red) shown in Figure 17, the consistencies of the designed gear ratio and the analyzed gear ratio were verified. Furthermore, the preciseness of the generating method and the generating mathematical model were also proven. The fluctuations of the blue curve is caused by FEM analysis which considering the dynamic of gear system.

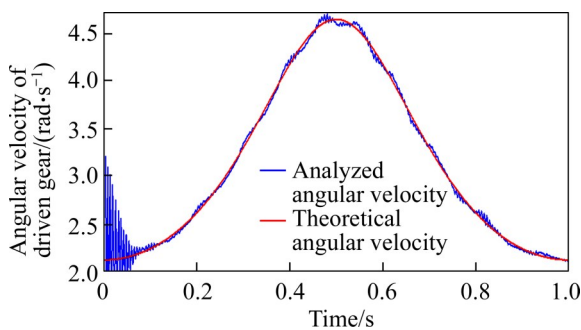


Figure 17 Angular velocity of driven gear

The contact areas of the drive gear on concave flanks and the contact areas of the driven gear on convex flanks over time are shown in Tables 5 and 6, respectively. The equivalent stress distributions of the drive gear and driven gear over time are shown in Tables 7 and 8, respectively. In addition, the evolutions of the maximum stress curves of these two contact gears over time are shown in Figure 18. The FEA results indicated that:

Table 5 Contact areas of drive gear on concave surfaces over time

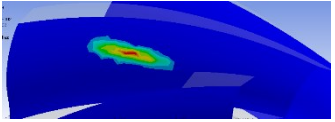
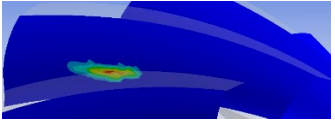
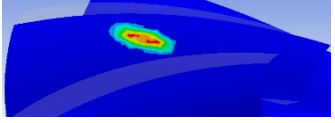
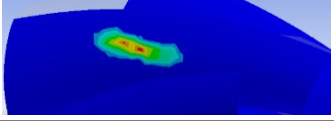
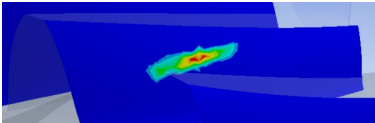
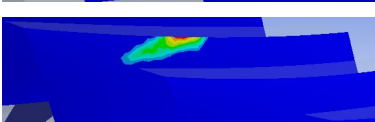
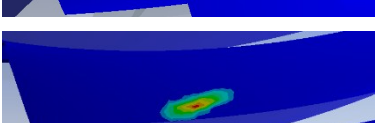
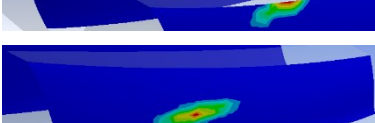
Time/s	Maximum contact pressure/MPa	Contact area
0.13476	155.02	
0.40333	424.60	
0.80330	219.24	
1.00000	148.81	

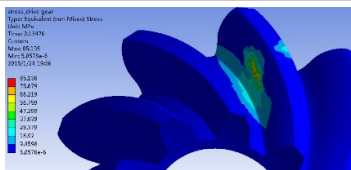
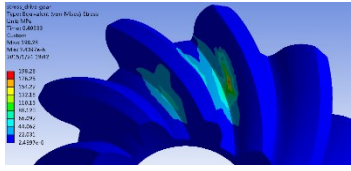
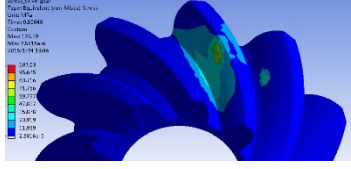
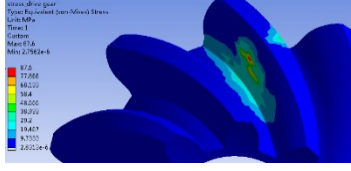
Table 6 Contact areas of driven gear on convex surfaces over time

Time/s	Maximum contact pressure/MPa	Contact area
0.13476	142.43	
0.40333	467.91	
0.80330	236.04	
1.00000	206.65	

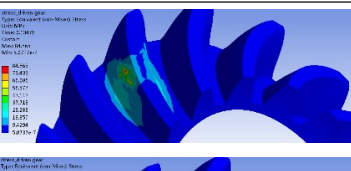
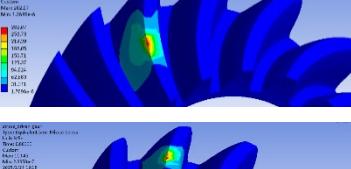
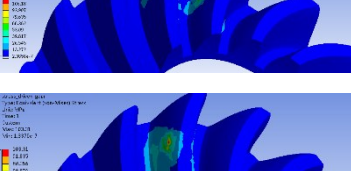
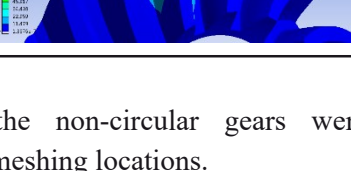
1) The bearing contact was stabilized, and the contact patterns were no different from those of the spiral bevel gears [37], indicating that the contact region adjustment method of spiral bevel gears could be applied to spiral non-circular bevel gears.

2) The contact area could be the result of one or two meshing teeth. The load was distributed among two or three pairs of meshing teeth since the

**Table 7** Equivalent stress of drive gear over time

Time/s	Maximum equivalent stress/MPa	Contact area
0.13476	85.138	
0.40333	198.280	
0.80330	107.630	
1.00000	87.600	

**Table 8** Equivalent stress of driven gear over time

Time/s	Maximum equivalent stress/MPa	Contact area
0.13476	84.865	
0.40333	282.070	
0.80330	199.450	
1.00000	103.310	

contact ratios of the non-circular gears were different at different meshing locations.

3) Edge contact was present at the top edges of the tooth surfaces of both the drive and driven gears. Thus, similar to spiral bevel gears, a tip relief

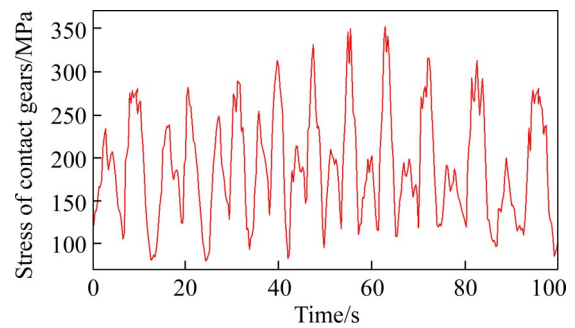


**Figure 18** Evolution of contact gears' maximum stress

should be applied in order to avoid these areas of severe contact stress.

4) The maximum stress evolution (Figure 18) was consistent with the angular velocity trend of the driven gear (Figure 17), but opposite to the gear ratio trend (Table 1). This suggested that the areas of severe contact stress appeared near the meshing position at the minimum gear ratio.

## 6 Conclusions

1) A spiral non-circular bevel gear with a high contact ratio, high intensity, excellent dynamic performance, and simple processing method compared to straight non-circular bevel gears was proposed by combining the generating methods of spiral bevel gears and the meshing theory of non-circular bevel gears.

2) Based on the generating principles and methods of spiral bevel gears, a mathematical model for spiral non-circular bevel gearing, including the tooth spiral, pressure angle, and tooth spiral, was discussed.

3) The mathematical model was successfully applied to the design of a pair of spiral non-circular bevel gears with 2-order sinusoidal gear ratio functions. According to the FEA analysis, the angular velocity of the driven gear was consistent with the theoretical angular velocity, confirming the precision of the mathematical model.

4) The FEA results indicated that the change in maximum stress was related to the transient gear ratio, and that the contact of the spiral non-circular bevel gear was no different than that of the spiral bevel gear in terms of their contact patterns and edge contacts.

## Nomenclature

$W$	Point width of the cutter blade
$\alpha_1$	Concave pressure angles of the cutter
$\alpha_2$	Convex pressure angles of the cutter
$e_p$	Distance of the cutter center to the machine center
$r_v$	Mean radius of the cutter
$r_{vd}$	Outer radius of the cutter
$r_{vx}$	Inner radius of the cutter
$r_f$	Mean cone distance
$\beta_f$	Mean spiral angle
$m_f$	Module of the flat-top generator
$A_o$	Pitch cone of noncircular bevel gear
$A_f$	Root cone of noncircular bevel gear
$A_a$	Face cone of noncircular bevel gear
$\varphi_0$	Rotating angle of non-circular bevel gear
$\delta_0$	Pitch angle of non-circular bevel gear
$\varphi_1$	Rotating angle of drive non-circular bevel gear
$\varphi_2$	Rotating angle of driven non-circular bevel gear
$i_{12}$	Gear ratio function
$\delta_1$	The pitch angle of drive non-circular bevel gear
$\delta_2$	The pitch angle of driven non-circular bevel gear
$m_F$	The mean module, or module on the mean pitch curve of noncircular bevel gear
$t_1$	Tangent vector of pitch cone in circumferential direction
$t_{1u}$	The unit tangent vector of pitch cone in circumferential direction
$t_2$	Tangent vector of the pitch cone in radial direction
$t_{2u}$	The unit tangent vector of pitch cone in radial direction
$n_{1u}$	Unit normal vector of the pitch cone
$A_p$	Face cone of the flat-top generator (a plane)
$t_{3u}$	Unit tangent vector of the root cone in circumferential direction
$t_{4u}$	Unit tangent vector of the root cone radial direction
$n_{3u}$	Unit normal vector of the root cone
$M_{ij}$	Homogeneous transformation matrix from coordinate system $S_j$ to coordinate system $S_i$
$i, j, k_i$	Base vector of coordinate system $S_i$
$\theta_p$	Angle of generator
$t_1, t_r$	Tangent vectors of the generator's tooth profile in two different directions
$n_r$	Normal vector of the generator's tooth profile
$v_c$	Relative velocity between the generator and generated gear
$\theta_p$	Angle of generator

## Contributors

HAN Xing-hui provided the concept and edited the draft of manuscript. ZHENG Fang-yan and TIAN Jun implemented the experiment and wrote the first draft of the manuscript. ZHANG Xuan-cheng and XU Man provided the experiment instrument and advised on the analysis of the experiment result.

## Conflict of interest

HAN Xing-hui, ZHANG Xuan-cheng, ZHENG Fang-yan, XU Man and TIAN Jun declare that they have no conflict of interest.

## References

- [1] LITVIN F L, GONZALEZ-PEREZ I, FUENTES A, et al. Design and investigation of gear drives with non-circular gears applied for speed variation and generation of functions [J]. *Computer Methods in Applied Mechanics and Engineering*, 2008, 197(45–48): 3783–3802.
- [2] OTTAVIANO E, MUNDO D, DANIELI G A, et al. Numerical and experimental analysis of non-circular gears and cam-follower systems as function generators[J]. *Mechanism and Machine Theory*, 2008, 43(8): 996–1008.
- [3] ZHENG Fang-yan, HUA Lin, HAN Xing-hui, et al. Generation of noncircular bevel gears with free-form tooth profile and curvilinear tooth lengthwise [J]. *Journal of Mechanical Design*, 2016, 138(6): 064501.
- [4] WU Yi-fei, GE Pei-qi, BI Wen-bo. Analysis of axial force of double circular arc helical gear hydraulic pump and design of its balancing device [J]. *Journal of Central South University*, 2021, 28(2) : 418–428.
- [5] TERADA H, ZHU Y, SUZUKI M, et al. Developments of a knee motion assist mechanism for wearable robot with a non-circular gear and grooved cams [M]. Netherlands: Springer 2012: 69–76.
- [6] MODLER K H, LOVASZ E C, NEUMANN R. General method for the synthesis of geared linkages with non-circular gears [J]. *Mechanism and Machine Theory*, 2009, 44(4): 726–738.
- [7] LUO Shan-ming, WU Yue, WANG Jian. The generation principle and mathematical models of a novel cosine gear drive [J]. *Mechanism and Machine Theory*, 2008, 43(12): 1543–1556.
- [8] MUNDO D. Geometric design of a planetary gear train with non-circular gears [J]. *Mechanism and Machine Theory*, 2006, 41(4): 456–472.
- [9] LIN Chao, HOU Yu-jie, GONG Hai, et al. Flow characteristics of high-order ellipse bevel gear pump [J]. *Journal of Drainage and Irrigation Machinery Engineering*, 2011, 29(5): 379–385. (in Chinese)
- [10] ZHENG Fang-yan, HUA Lin, HAN Xing-hui, et al. Synthesis of shaped noncircular gear using a three-linkage

- computer numerical control shaping machine [J]. *Journal of Manufacturing Science and Engineering*, 2017, 139(7): 071003.
- [11] ZHENG Fang-yan, HUA Lin, HAN Xing-hui. The mathematical model and mechanical properties of variable center distance gears based on screw theory [J]. *Mechanism and Machine Theory*, 2016, 101: 116–139.
- [12] CHEN Ming-zhang, XIONG Xiao-shuang, ZHUANG Wu-hao. Design and simulation of meshing performance of modified straight bevel gears [J]. *Metals*, 2021, 11(1): 33.
- [13] OLLSON U. Non circular bevel gears [M]. Stockholm, Sweden: the Royal Swedish Academy of Engineering Sciences, 1959.
- [14] XIE Xia, ZHANG Xiao-bao, JIA Ju-min, et al. Coordinate measuring of the variable ratio noncircular bevel gear [C]// *International Conference on Electronic and Mechanical Engineering and Information Technology*. IEEE, 2011: 4471–4473.
- [15] LIN Chao, HOU Yu-jie, GONG Hai, et al. Design and analysis of transmission mode for high-order deformed elliptic bevel gears [J]. *Journal of Mechanical Engineering*, 2011, 47(13): 131–131.
- [16] LIN Chao, ZHANG Lei, ZHANG Zhi-hua. Transmission theory and tooth surface solution of a new type of non-circular bevel gears[J]. *Journal of Mechanical Engineering*, 2014, 50(13): 66–72. (in Chinese)
- [17] LI Hai-tao, WEI Wen-jun, LIU Ping-yi, et al. The kinematic synthesis of involute spiral bevel gears and their tooth contact analysis [J]. *Mechanism and Machine Theory*, 2014, 79: 141–157.
- [18] LITVIN F L, FUENTES A, HAYASAKA K. Design, manufacture, stress analysis , and experimental tests of low-noise high endurance spiral bevel gears [J]. *Mechanism and Machine Theory*, 2006, 41(1): 83–118.
- [19] MU Yan-ming, HE Xue-ming. Design and dynamic performance analysis of high-contact-ratio spiral bevel gear based on the higher-order tooth surface modification [J]. *Mechanism and Machine Theory*, 2021, 161: 104312.
- [20] ZHENG Fang-yan, ZHANG Ming-de, ZHANG Wei-qing, et al. The fundamental roughness model for face-milling spiral bevel gears considering run-outs [J]. *International Journal of Mechanical Sciences*, 2019, 156(C): 272–282.
- [21] YANG Zhao-jun, HONG Zhao-bin, WANG Bai-chao, et al. New tooth profile design of spiral bevel gears with spherical involute [J]. *International Journal of Advancements in Computing Technology*, 2012, 4(19): 462–469.
- [22] ALVES J T, GUINGAND M, VAUJANY J D. Designing and manufacturing spiral bevel gears using 5-axis computer numerical control (cnc) milling machines [J]. *Journal of Mechanical Design*, 2013, 135(2): 024502–024507.
- [23] LIN Chung-yun, TSAY Chung-biau, FONG Zhang-hua. Computer-aided manufacturing of spiral bevel and hypoid gears by applying optimization techniques [J]. *Journal of Materials Processing Technology*, 2001, 114(1): 22–35.
- [24] LIN Jing. Tooth surface generation and geometric properties of straight noncircular bevel gears [J]. *Journal of Mechanical Design*, 2012, 134(8): 084503.
- [25] ZHAO Ya-ping, KONG Xiang-wei. Meshing principle of conical surface enveloping spiroid drive [J]. *Mechanism and Machine Theory*, 2018, 123: 1–26.
- [26] LITVIN F L, TUNG WEIJIUNG, COY J J. Method for generation of spiral bevel gears with conjugate gear tooth surfaces [J]. *Journal of Mechanisms Transmissions and Automation in Design* 1987, 109(6): 163–170.
- [27] LITVIN F L, GONZALEZ-PEREZ I, YUKISHIMA K, et al. Generation of planar and helical elliptical gears by application of rack-cutter, hob, and shaper [J]. *Computer Methods in Applied Mechanics and Engineering*, 2007, 196(41–44): 4321–4336.
- [28] LITVIN F L, FUENTES A. Gear geometry and applied theory [M]. Cambridge: Cambridge University Press, 2008.
- [29] LIN Chao, GONG Hai, HOU Yu-jie, et al. Tooth profile design and manufacture of higher-order elliptical bevel gears [J]. *China Mechanical Engineering* 2012, 23(3): 253–258. (in Chinese)
- [30] LITVIN F L. Gear geometry and applied theory [J]. *Mechanism and Machine Theory*, 1995, 30(3): 36–44.
- [31] SIMON V. Head-cutter for optimal tooth modifications in spiral bevel gears [J]. *Mechanism and Machine Theory*, 2009, 44(7): 1420–1435.
- [32] FUENTES A, LITVIN F L, MULLINS B R, et al. Design and stress analysis, and experimental tests of low-noise adjusted bearing contract spiral bevel gears [J]. *VDI-Berichte*, 2002, 1665: 327–340.
- [33] ARTONI A, GABICINI M, KOLIVAND M. Ease-off based compensation of tooth surface deviations for spiral bevel and hypoid gears: Only the pinion needs corrections [J]. *Mechanism and Machine Theory*, 2013, 61: 84–101.
- [34] ZHENG Fang-yan, HUA Lin, HAN Xing-hui. Non-uniform flank rolling measurement for shaped noncircular gears [J]. *Measurement*, 2017: S0263224117304876.
- [35] DOONER D B, SEIREG. The kinematic geometry of gearing [M]. New York: John Wiley and Sons, 1995: 80–81.
- [36] BAIR B W, SUNG M H, WANG J S, et al. Tooth profile generation and analysis of oval gears with circular-arc teeth [J]. *Mechanism and Machine Theory*, 2009, 44: 1306–1317.
- [37] JOHN A, ALFONSO F, FAYDOR L. Computerized integrated approach for design and stress analysis of spiral bevel gears [J]. *Computer Methods in Applied Mechanics and Engineering*, 2002, 191(11, 12): 1057–1095.

(Edited by YANG Hua)

## 中文导读

### 新型螺旋非圆锥齿轮的数学模型和齿面接触分析

**摘要：** 本文结合非圆锥齿轮的设计原理和面铣螺旋锥齿轮的制造原理，提出了一种可应用于相交轴变速传动的新型螺旋非圆锥齿轮。与直齿非圆锥齿轮不同，螺旋非圆锥齿轮有许多优点，如高接触比、高强度、良好的动态性能和可调节的接触区域。此外，虽然制造直齿非圆锥齿轮很困难，但螺旋非圆锥齿轮可以用6轴锥齿轮切削机床高效、精确地制造。首先，介绍了螺旋非圆锥齿轮的产形原理。接着，建立了一个数学模型，包括产形齿的齿廓、齿轮螺旋度、压力角和该齿轮的产形齿廓。然后，利用有限元进行齿轮接触分析，验证了模型精度，并研究了螺旋非圆锥齿轮的接触模式和应力分布。

**关键词：** 非圆形齿轮；螺旋锥齿轮；数学模型；齿轮接触分析